A 648 x 484-Pixel 4-Tap Hybrid Time-of-Flight Image Sensor with 8 and 12 Phase Demodulation for Long-Range Indoor and Outdoor Operations

Kamel Mars[1], Kensuke Sakai[1], Yugo Nakatani[1], Masashi Hakamata[1], Keita Yasutomi[1], De Xing Lioe[1], Keiichiro Kagawa[1], Tomoyuki Akahori[2], Tomohiko Kosugi[2], Satoshi Aoyama[2], Shoji Kawahito[1,2]
[1] : Research Institute of Electronics, Shizuoka University, Hamamatsu, 432-8011, Japan
[2] : Brookman Technology, Inc., Hamamatsu, 430-0936, Japan
email: kamel@idl.rie.shizuoka.ac.jp **TEL**: +81-53-478-1341 **FAX**: +81-53-478-3251

I. Introduction

For 3D depth sensing, direct ToF (dToF) sensors are becoming popular particularly for long-range outdoor applications, but the dToFs has a difficulty of high depth-image resolution if high ambient light operation is required [1]-[3]. On the other hand, indirect TOF (iTOF) image sensors using Continuous-Wave (CW) demodulation pixels are good solution for high image resolution ToF cameras [4]-[7], but the iToFs have a difficulty of long-range measurements under strong ambient light because the iToF pixels using 50% duty-cycle operation suffer from strong ambient light. This paper presents a 100klux ambient light tolerant VGA-resolution hybrid-type ToF image sensor, which is basically a short-pulse (SP) based iToF but practically uses a concept of the dToF for finding the received light-pulse location as a digital number in the multiple time windows prepared by multi-tap pixel outputs and multiple subframes [8-9]. The presented hybrid ToF technique has distinct advantages over the CW-iTOF counterpart because of the reduced in-pixel ambient-light charge acquisition and the resulting small amount of ambient-light shot noise for outdoor operation.

II. Sensor Architecture and Operation

Figure 1 shows the sensor chip architecture and 4-tap demodulation pixel with a lateral-drift pinned-photo diode structure and lateral electric-field control gates, G1~G4 and drain gate GD. Fast driving of MOS gates can be achieved using a shared in-pixel driver with two driver circuits (i.e. Top and bottom driver) where each of them is used for one half of the pixel array for better drivability. In a pixel pitch of 16.8um, 4PGAs (4.2um pitch) and 4 succeeding 12b cyclic A/D converter

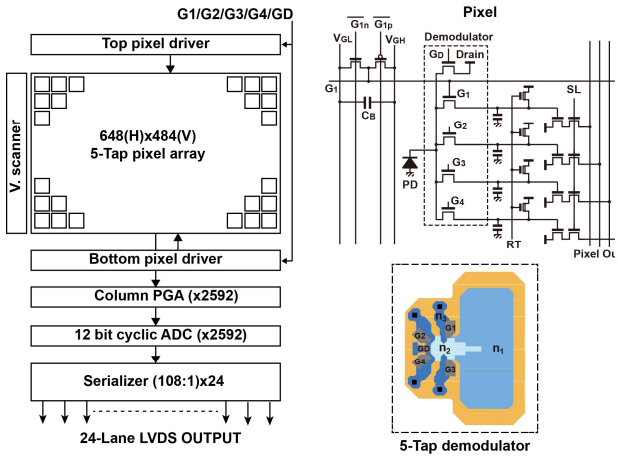

Figure 1: Prototype chip photograph (Left), Pixel circuit and demodulator diagram (Right).

(4.2um pitch) are arranged at the column allowing a fully-parallel readout of 4-taps per pixel. With 24 serializers (108-to-1), and 24-lane LVDS outputs, the TOF image data are readout at maximally 11.5Gbps ensuring a fast readout time of the full 4-tap VGA images in just 1.45ms allowing a higher frame rate to be achieved using hybrid-type ToF measurements.

In order to exploit the feature of the SP modulation method while attaining wide distance measurement range, the proposed method uses multiple time-gating pulses and range-shifted TOF measurements with multiple sub-frame (SF) readouts as shown in Figure 2 and Figure 3 for both indoor and outdoor operation respectively. Outdoor operation as depicted by the timing diagram in Figure 3, uses four subframes, where the first two are used for the near depth zone and the other two are used for far depth zone. By using 8 gating pulses, a measurable range of 0 to 7TP (e. g., 11.8m for TP of 11.25ns, where TP is the light-pulse width) is

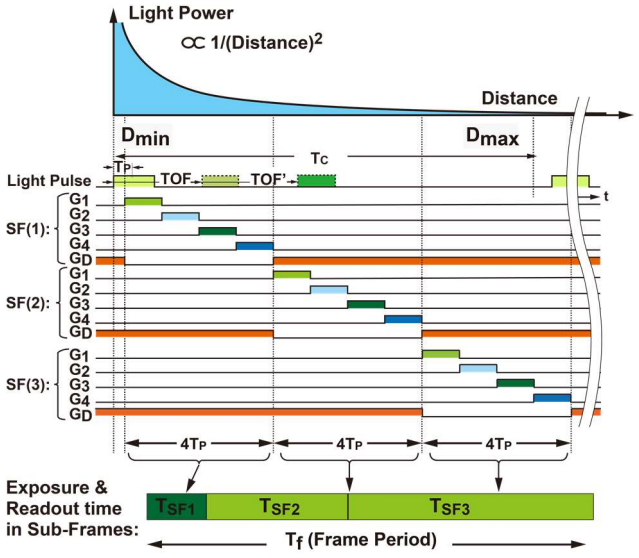

Figure 2: 3-subframes gates timing chart for indoor measurement

attained by a careful selection of the exposure time ratio based on the fact that light power attenuation is inversely proportional to the square of the distance. Two sub-frame readouts with switching gate pulses between G1 and G3, or G2 and G4 for each depth zone as shown in Figure 3 are used with the aim of reducing ambient light-induced depth offset when a tap-to-tap conversion gain deviation is considered. By calculating the difference of two signals of SF(1) to SF(2) and SF(3) to SF(4), signal components are added while the residual ambient-light offset components due to the tap-to-tap gain deviation are canceled out.

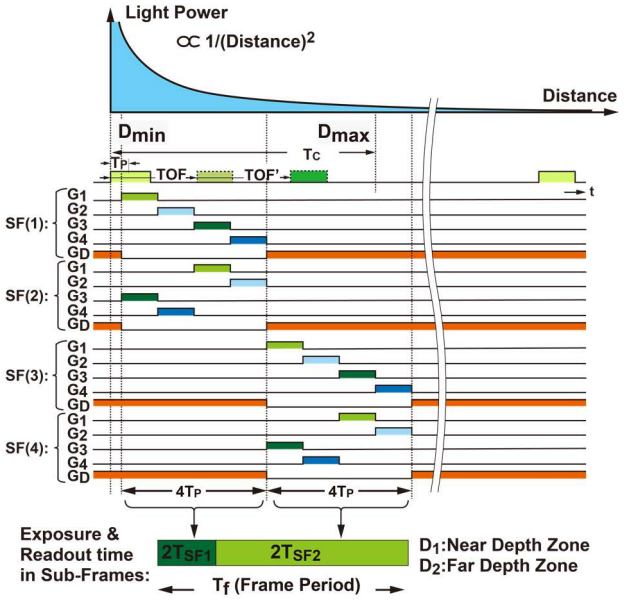

Figure 3: 4-subframes gates timing chart for outdoor measurement

The output signal of *i*th tap, S_i if the conversion gain is deviated from tap to tap can be expressed as

$$S_i = (G + \Delta G_i)(X_{Sk} + X_{Ak}) \quad (1)$$

where X_{Sk} is the signal charge generated at *k*th gate timing, X_{Ak} is the ambient light charge generated at *k*th gate timing, G is the conversion gain factor and ΔG_i is the deviation of G. Based on the timing chart of the outdoor operation, the signal differences in the first subframe, $S_{13} = S_1 - S_3$ and $S_{24} = S_2 - S_4$ can be expressed as

$$S_{13}^{SF} = (G + \Delta G_1)(X_{S1}^{SF1} + X_{A1}^{SF1}) - (G + \Delta G_3)(X_{S3}^{SF1} + X_{A3}^{SF1}) \quad (2)$$

and

$$S_{24}^{SF1} = (G + \Delta G_2)(X_{S2}^{SF1} + X_{A2}^{SF}) - (G + \Delta G_4)(X_{S4}^{SF} + X_{A4}^{SF1}). \quad (3)$$

Since the order of tap opening is being inverted in the second subframe, $S_{13} = S_1 - S_3$ and $S_{24} = S_2 - S_4$ can be expressed as

$$S_{13}^{SF2} = (G + \Delta G_1)(X_{S3}^{SF2} + X_{A3}^{SF2}) - (G + \Delta G_3)(X_{S1}^{SF} + X_{A1}^{SF2}) \quad (4)$$

and

$$S_{24}^{SF2} = (G + \Delta G_2)(X_{S4}^{SF} + X_{A4}^{SF2}) - (G + \Delta G_4)(X_{S2}^{SF} + X_{A2}^{SF2}). \quad (5)$$

Since gates opening time is set to be the same, and careful exposure time setting and fast readout time are performed, we can assume that in each subframe, the ambient light components of each tap are equal, i.e., $X_{A1}^{SF} = X_{A3}^{SF} \equiv X_A^{SF}$ and $X_{A1}^{SF2} = X_{A3}^{SF2} \equiv X_A^{SF2}$. Equations (2) and (4) can be simplified by the following two equations:

$$S_{13}^{SF1} = G(X_{S1}^{SF} - X_{S3}^{SF1}) + \Delta G_1 X_{S1}^{SF1} - \Delta G_1 X_{S3}^{SF1} + (\Delta G_1 - \Delta G_3) X_A^{SF} \quad (6)$$

and

$$S_{13}^{SF2} = G(X_{S3}^{SF2} - X_{S1}^{SF2}) + \Delta G_1 X_{S3}^{SF} - \Delta G_1 X_{S1}^{SF2} + (\Delta G_1 - \Delta G_3) X_A^{SF} \quad (7)$$

The deviation factor due to ambient light in the first and second subframe ΔS_A^{SF1} and ΔS_A^{SF2} can be expressed as follow:

$$\Delta S_A^{SF} = (\Delta G_1 - \Delta G_3) X_A^{SF} \quad (8)$$

and

$$\Delta S_A^{SF2} = (\Delta G_1 - \Delta G_3) X_A^{SF2} \quad (9)$$

By taking the difference of two signal component of the first and second subframe ($S_{13} = S_{13}^{SF1} - S_{13}^{SF2}$), the deviation factor can be express as

$$\Delta S_A^{SF12} = (\Delta G_1 - \Delta G_3)(X_A^{SF1} - X_A^{SF}) \quad (10)$$

Equations 6 to 10 show that the signal component can be doubled while the ambient light component is canceled out and taps deviation is being minimized by calculating the difference of two subframes signals if background scene is not largely changed during the two subframes.

The same procedure is also used for tap 2 and 4 and performed for the far range (i.e. subframes 3 and 4) too.

For indoor operations where the background ambient light is not strong, 3 SFs are used as shown by the timing chart depicted in Figure 2 and 12 successive gating pulses can be used for 20m-range measurements of 0 to 11TP (i.e. 18.56m for TP of 11.25ns).

III. MEASURMENT RESULTS

In order to measure the proposed design, a prototype chip where the photomicrograph is shown in Figure 4 has been fabricated using 0.11um COMS image sensor process. Table 1 shows a summary of specifications and basic characteristics of the chip. Figure 5 shows the measured response curve of the 3-subframes (Top) and 4-subframes (bottom) time-gating to the delay of light pulse. In 4-subframes case intended to be used for outdoor operation, only difference of two signals of SF(1) to SF(2) and SF(3) to SF(4) is depicted.

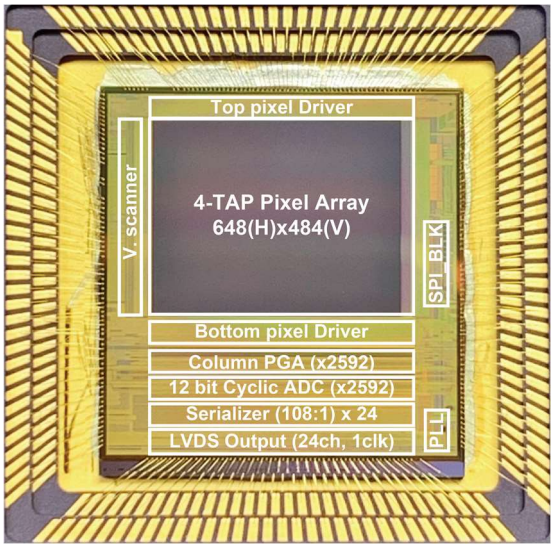

Figure (4): Prototype chip micro-photograph

Table 1: Summary of the prototype CMOS imager performance

Parameter	value
Technology	0.11µm CMOS Image sensor
Number of Pixels	648 (H) × 480 (V)
Pixel size	16.8 µm × 16.8 µm
Chip size	14.92 mm × 15.5 mm
ADC resolution	12 bits cyclic
Readout time	1.45 ms (12 bit)
Conversion gain	10.0 µV/e$^-$
Quantum Efficiency	18.6 % @(940 nm)

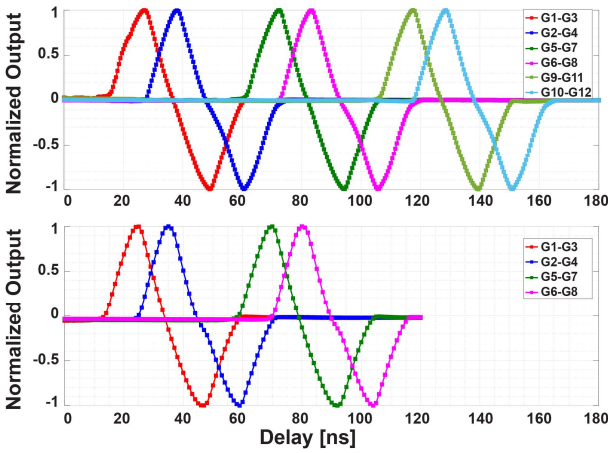

Figure 5: Pixel response to the light-pulse delay: 3-zone curves (top) and 2-zone curves (bottom).

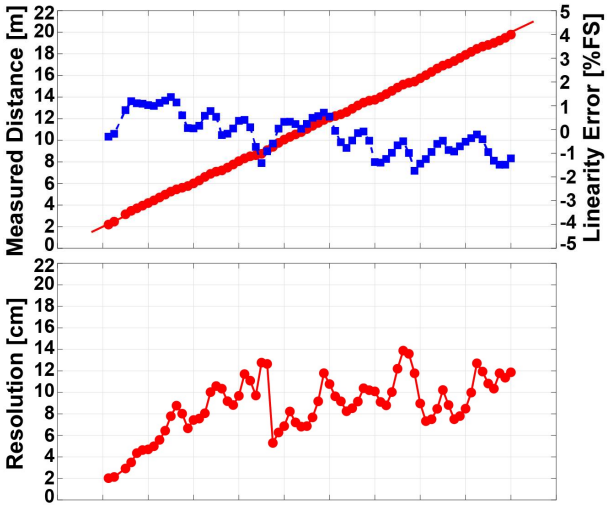

Figure 6: Indoor Distance, linearity and depth-noise measurements.

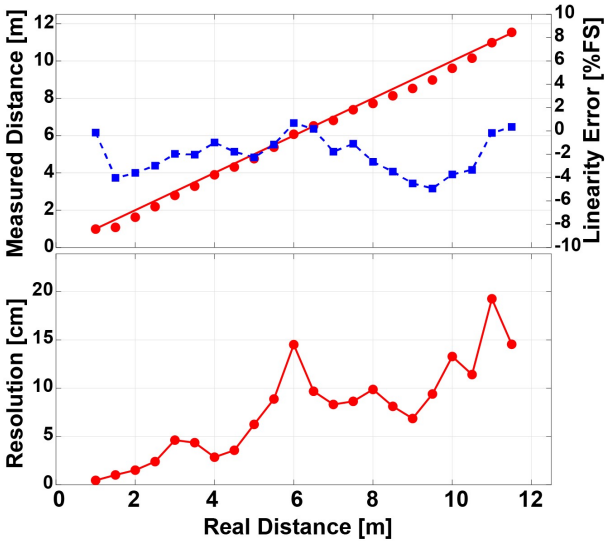

Figure 7: Outdoor distance, linearity and depth-noise measurement under 100klx

Figure 6 and Figure 7 shows the measured distance, linearity and depth noise (precision) for indoor (2-20m), and outdoor (1 to 11.5m) respectively. In the indoor measurements as depicted in Figure 6, the maximum non-linearity is 2%, and the maximum depth noise is 1.7% in the entire distance range. At 20m, a depth noise of 0.6% is attained. On the other hand, in the outdoor measurements as depicted in Figure 7, the maximum non-linearity is 4% and the depth noise at 10m is 1.6%. For both indoor and outdoor operation, the light pulse width and gates pulse with was set to 11ns and sensitivity correction between taps has been performed. Figure 8 shows the captured depth images for indoor (20m) and outdoor (10m, 110klux) measurements.

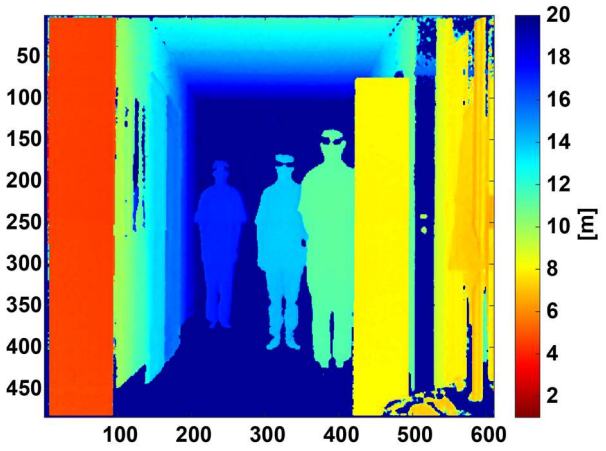

(a)

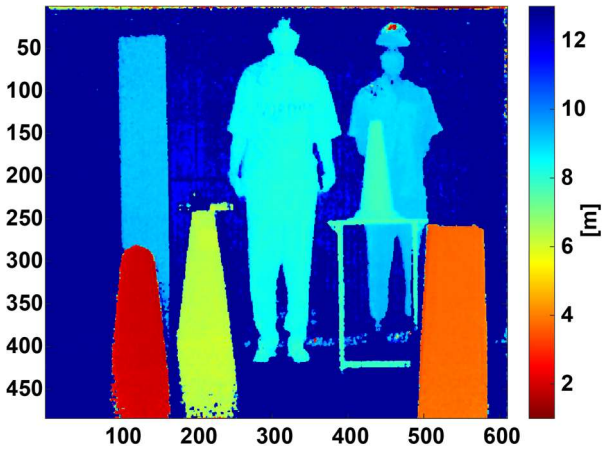

(b)

Figure 8: Captured TOF Images: (a) Indoor, (b) outdoor

ACKNOWLEDGMENT

This work was partly supported by Adaptable and Seamless Technology Transfer Program through Target-driven R&D (A-STEP) from Japan Science and Technology Agency (JST) Grant Number JPMJTR211A. It was also partly supported by A JSPS KAKENHI Grand Number 18H05240, 19H02194, and the Center of Innovation Program. The authors also appreciate DB HiTek for the prototype chip fabrication.

REFERENCES

[1] H. Seo et al., "Direct TOF Scanning LiDAR Sensor With Two-Step Multievent Histogramming TDC and Embedded Interference Filter," in IEEE Journal of Solid-State Circuits, vol. 56, no. 4, pp. 1022-1035, April 2021.

[2] B. Kim, S. Park, J. -H. Chun, J. Choi and S. -J. Kim, "7.2 A 48×40 13.5mm Depth Resolution Flash LiDAR Sensor with In-Pixel Zoom Histogramming Time-to-Digital Converter," in IEEE ISSCC Dig. Tech. Papers, Feb. 2021, pp. 108–110.

[3] O. Kumagai et al., "A 189 × 600 back-illuminated stacked SPAD direct time-of-flight depth sensor for automotive LiDAR systems," in IEEE ISSCC Dig. Tech. Papers, Feb. 2021, pp. 110–111.

[4] C. S. Bamji et al., "1Mpixel 65nm 320MHz demodulated TOF image sensor with 3.5um global shutter pixels and analog binning," in IEEE ISSCC Dig. Tech. Papers, Feb. 2018, pp. 94–95.

[5] M.-S. Keel et al., "A 4-tap 3.5μm 1.2Mpixel indirect time-of- flight CMOS image sensor with peak current mitigation and multi-user interference cancellation," in IEEE ISSCC Dig. Tech. Papers, Feb. 2021, pp. 105–106.

[6] D. Kim et al., "Indirect time-of-flight CMOS image sensor with on-chip background light cancelling and pseudo-four-tap/two-tap hybrid imaging for motion artifact suppression," IEEE J. Solid-State Circuit, vol. 55, no. 11, pp. 2849–2865, Nov. 2020.

[7] Y. Ebiko et al., "Low power consumption and high resolution 1280x960 gate assisted photonic demodulator pixel for indirect time of flight," in Int. Electron Device Meeting Tech. Dig., Dec. 2020, pp. 721–724.

[8] K. Hatakeyama et al., "A hybrid indirect ToF image sensor for long-range 3D depth measurement under high ambient light conditions," in Proc. IEEE Symp. VLSI Technol. Circuits, Jun. 2022, pp. 46–47

[9] S. Kawahito, K. Yasutomi and K. Mars, "Hybrid Time-of-Flight Image Sensors for Middle-Range Outdoor Applications," in IEEE Open Journal of the Solid-State Circuits Society, vol. 2, pp. 38-49, 2022